Hyperpolarized ^{13}C Magnetic Resonance Imaging Can Detect Metabolic Changes Characteristic of Penumbra in Ischemic Stroke

Yafang Xu, Steffen Ringgaard, Christian Østergaard Mariager, Lotte Bonde Bertelsen, Marie Schroeder, Haiyun Qi, Christoffer Laustsen, and Hans Stødkilde-Jørgensen

Department of Clinical Medicine, MR Research Centre, Aarhus University, Aarhus, Denmark

Corresponding Author:
Hans Stødkilde-Jørgensen, MD, DMSc
Palle Juul-Jensens Boulevard 99, 8200 Aarhus N, Denmark;
E-mail: hsj@clin.au.dk

Key Words: MRI, hyperpolarized 13C, cerebral stroke, endothelin-1
Abbreviations: Magnetic resonance imaging (MRI), adenosine triphosphate (ATP), magnetic resonance (MR), endothelin-1 (ET-1), blood–brain barrier (BBB), lactate dehydrogenase (LDH), monocarboxylate transporters (MCT)

ABSTRACT

Magnetic resonance imaging (MRI) is increasingly the method of choice for rapid stroke assessment in patients and for guiding patient selection in clinical trials. The underlying metabolic status during stroke and following treatment is recognized as an important prognostic factor; thus, new methods are required to monitor local biochemistry following cerebral infarction, rapidly and in vivo. Hyperpolarized MRI with the tracer [1-^{13}C]pyruvate enables rapid detection of localized [1-^{13}C]lactate production, which has recently been shown in patients, supporting its translation to assess clinical stroke. Here we show the ability of hyperpolarized ^{13}C MRI to detect the metabolic alterations characteristic of endothelin-1-induced ischemic stroke in rodents. In the region of penumbra, determined via T2-weighted ^{1}H MRI, both [1-^{13}C]pyruvate delivery and [1-^{13}C]pyruvate cellular uptake independently increased. Furthermore, we observed a 33% increase in absolute [1-^{13}C]lactate signal in the penumbra, and we determined that half of this increase was due to increased intracellular [1-^{13}C]pyruvate supply and half was mediated by enhanced lactate dehydrogenase-mediated [1-^{13}C]lactate production. Future work to characterize the kinetics of delivery, uptake, and enzymatic conversions of hyperpolarized tracers following ischemic stroke could position hyperpolarized ^{13}C MRI as an ideal technology for rapid assessment of the penumbra during the critical time window following ischemic stroke in patients.

INTRODUCTION

Stroke is the third leading cause of death worldwide and the leading cause of disability among adults. In total, 80% of strokes are ischemic, resulting from occlusion of a cerebral artery that deprives the tissue perfused by that artery of metabolic substrates and oxygen it requires to sustain function (1). The only Food and Drug Administration-approved therapy for ischemic stroke involves reperfusion by thrombolysis induced by intravenous injection of recombinant tissue plasminogen activator within 4.5 hours of ischemia onset (2). Mechanical clot retrieval has been shown to extend the treatment window to 6 hours in patients with stroke (3). There remains an urgent need to both develop new neuroprotective strategies that preserve tissue viability following ischemic stroke and further lengthen the treatment window during which patients can hope to receive successful treatment (4).

Experimental work on the flow thresholds of brain tissue showed the existence of the following 2 critical levels of decreased perfusion (5, 6): a level representing the flow threshold for reversible neuronal failure and a lower threshold below which irreversible morphological damage, adenosine triphosphate (ATP) depletion, and ultimately necrotic cell death occur. The tissue experiencing perfusion at rates between these limits is called the "ischemic penumbra," and it is characterized by the potential for functional recovery without morphological damage, provided that local blood flow can be reestablished within a certain time window (6). Biochemically, the penumbra is defined by high rates of glucose extraction and anaerobic glycolysis (7, 8), which generate lactate and small amounts of ATP that enable basic neuronal "housekeeping" functions temporarily (such as axonal transport, biosynthetic processes, and other functions not directly related to action potentials). The penumbra progressively experiences irreversible damage at a rate inversely proportional to residual blood flow, and within ~8–24 hours, it will be converted into a necrotic core unless reperfusion therapy is performed (6).

Therapy for a patient with ischemic stroke critically depends on the presence of a penumbra, as the penumbra is the only damaged tissue with potential to be rescued to restore cerebral function. Neuroimaging techniques that can be applied in the clinic to rapidly assess the penumbra are essential to guide treatment decisions and develop new therapies (6, 9). The combination of perfusion and diffusion-weighted magnetic resonance imaging (MRI) has emerged as one candidate (10); however, the MRI perfu-

ISSN 2379-1381 http://dx.doi.org/10.18383/j.tom.2017.00106

sion–diffusion mismatch tends to overestimate the penumbra size (11, 12). The inaccuracy of this marker may have had a role in the failures of numerous reperfusion and neuroprotective therapies at the clinical trial stage (13, 14).

A primary characteristic distinguishing penumbra from healthy tissue and necrotic core is elevated lactate production and concomitant acidosis due to the penumbra's reliance on anaerobic glycolysis for energy production (7, 15-17). Furthermore, increased lactate concentration in the penumbra is a well-established biomarker of tissue destruction (6-8, 15-18), with numerous studies suggesting that lactate concentrations exceeding 15 mmol/kg predict the development of irreversible tissue damage (15, 17). The increased signal-to-noise ratio inherent to an emerging imaging technique, that is, MRI using hyperpolarized ^{13}C-labeled contrast media, implies that, for the first time, noninvasive imaging of lactate levels may be possible in patients within a clinically relevant scan time (19-22). In the heart, liver, kidney and also in tumor tissue, hyperpolarized ^{13}C magnetic resonance (MR) methods showed sensitivity to pathologically elevated lactate production (20, 22-26), upon infusion of the tracer hyperpolarized [1-^{13}C]pyruvate. Furthermore, although pyruvate uptake is limited by the blood–brain barrier (BBB) (27), sufficient [1-^{13}C]pyruvate has been shown to reach the cerebral tissue via the saturable monocarboxylate transporters (MCT1 and MCT2) and nonsaturable processes to enable metabolic imaging of the organ (28, 29). Imaging of the metabolic fate of hyperpolarized [1-^{13}C]pyruvate could effectively assess the penumbra noninvasively, to report on the penumbra volume and to predict risk of irreversible damage before reperfusion, via detection of [1-^{13}C]lactate distribution and signal intensity.

The aim of this study is to provide a proof-of-concept that hyperpolarized ^{13}C MRI can delineate the penumbra in patients with ischemic stroke on the basis of imaging-localized [1-^{13}C]lactate production. Our results achieved this aim, and, in addition, showed the surprising results that hyperpolarized MRI with [1-^{13}C]pyruvate can inform upon regional, independent alterations to perfusion and cellular uptake. The work will provide the foundation for studies using hyperpolarized ^{13}C MRI to guide management of patients with stroke and facilitate the validation of new clinical therapies.

METHODS AND MATERIALS

In this study, 8-week-old male Sprague–Dawley rats (n = 6; weight, 350–410 g) were used. This study complied with the guidelines for use and care of laboratory animals and was approved by the Danish Inspectorate of Animal Experiments (2012-15-2934-00581).

Animal Handling

Before surgery, all the rats were housed under a 12:12 light:dark cycle with free access to water and rodent chow. The animals were anesthetized initially with 3% sevoflurane in 2 L/min air. The animals underwent the following surgical procedure that used endothelin-1 (ET-1) dissolved in sterile saline, as previously described (30, 31). Throughout the procedure, their temperature was maintained between 36.5°C and 37.5°C using a heating blanket.

In brief, animals were placed in a stereotaxic apparatus, a midline incision was made, and small burr holes were drilled at the coordinates given below. Every rat was given 2 cortical injections of 400 pmol ET-1 each, in a volume of 2 μL for each injection, using a 10-μL Hamilton Syringe. The stereotaxic coordinates for the first injection were anteroposterior, 0.0 mm; mediolateral, −2.5 mm; and dorsoventral, −2.3 mm; for the second injection, the stereotaxic coordinates were anteroposterior, +2.3 mm, mediolateral, −2.5 mm, and dorsoventral −2.3 mm. All stereotaxic measurements are relative to bregma, with depth determined from the skull surface. The incision was closed with nylon suture, and each rat was placed in a warm, dry recovery area with free, easy access to soft food and water.

Eighteen hours after induction of the ET-1 stroke, each rat was anesthetized once again and a tail vein catheterization was performed. Each rat was placed in a 3 T preclinical MR system (GE Healthcare, Brøndby, DK) equipped with a dual-tuned ^{1}H/^{13}C volume transmit–receive rat radiofrequency coil (GE Healthcare, Waukesha).

Hyperpolarization

One hundred and twenty seven mg of [1-^{13}C]pyruvic acid mixed with 15mM of the electron source AH111501 was polarized in a 5 T SPINLab (GE Healthcare, Brøndby, DK) to a reproducible polarization level of >40%, with a final concentration of 125mM. The hyperpolarized sample was manually transferred to the MR system in <30 seconds and injected in 15 seconds on average.

MRI Data Acquisition

An axial and coronal T2-weighted fast spin echo sequence was performed to scout for the hyperpolarized scan and to identify the stroke area. The sequence parameters include field of view = 80 × 80 mm^2, number of points = 320 × 320 (interpolated to 512 × 512), averages = 16, sections = 20, section thickness covering the brain = 2 mm, echo time = 80 milliseconds, and echo train = 20, with spectral width = 31.25 kHz and repetition time = 6 seconds. ^{13}C prescan optimization was performed on a ^{13}C-urea phantom (2 M) with an automated Bloch–Siegert phase-shift method to calibrate ^{13}C power. An axial section-selective ^{13}C IDEAL spiral sequence with a section thickness of 10 mm was used for hyperpolarized [1-^{13}C]pyruvate imaging, acquiring images every 5 seconds initiated 20 seconds after the start of injection. The sequence was run with a flip angle of 10°, 12 echoes (11 IDEAL echoes and 1 initial Free induction decay (FID) acquisition per IDEAL encoding), repetition time/echo time/Δecho time = 100 milliseconds/0.9 milliseconds/0.9 milliseconds, and field of view = 80 × 80 mm^2.

Image Analysis

Analysis of the hyperpolarized data was performed in vendor-delivered Matlab (MathWorks, Natick, MA) package and transferred to Osirix for region-of-interest analysis.

RESULTS AND DISCUSSION

^{1}H MR images revealed areas of visually apparent hyperintense areas of edema, characteristic of stroke on T2-weighted images, in 6 rats (Figure 1). The mean area of cerebrum affected by the stroke was 14.0 ± 2.10 mm^2, measured on the central section through the brain. The success rate of the ET-1 stroke procedure and the variability in resultant infarct size were in line

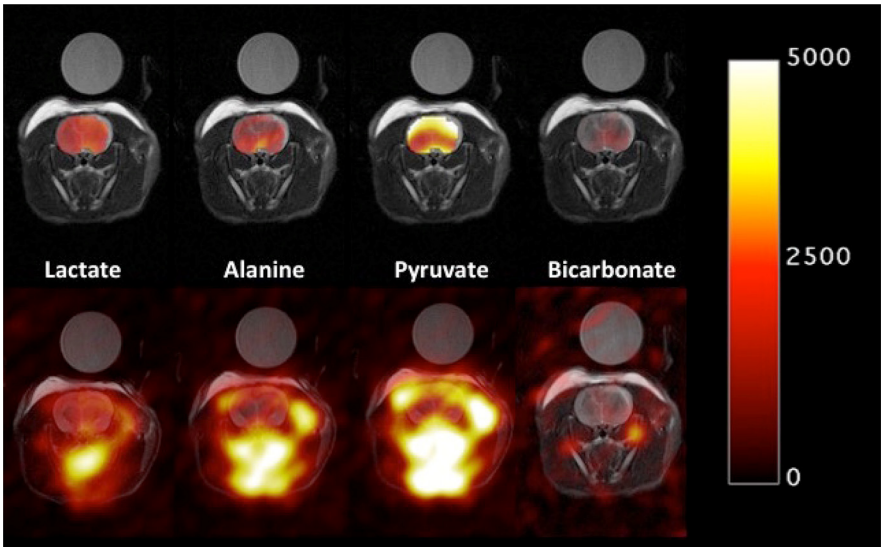

Figure 1. Representative ^{1}H and ^{13}C images acquired from the rodent brain, 18 hours after endothelin-1 (ET-1)-induced stroke. Top row: Cropped ^{13}C metabolite images overlaying the ^{1}H images. Bottom row: Uncropped ^{13}C metabolite images overlaying the ^{1}H images. All images are displayed with similar image scaling parameters.

with previous analyses of this method (30). In the 6 rats showing T2-weighted MRI evidence of ischemic stroke, the metabolic conversions of [1-^{13}C]pyruvate were assessed, comparing the region assigned as stroke to a remote region on the opposite hemisphere of the brain of comparable area and location.

Initially, to examine the metabolic changes inherent to the penumbra, we examined changes in the [1-^{13}C]lactate-to-[1-^{13}C]pyruvate, ^{13}C-bicarbonate-to[1-^{13}C]pyruvate, and [1-^{13}C]alanine-to-[1-^{13}C]pyruvate ratios between the stroke and remote regions. This is the most common method of normalizing metabolite signals for differences in tracer polarization and delivery. No alterations were observed in the [1-^{13}C]lactate-to[1-^{13}C]pyruvate or in the ^{13}C-bicarbonate-to-[1-^{13}C]pyruvate ratios, whereas the [1-^{13}C]alanine-to-[1-^{13}C]pyruvate ratio significantly reduced (Figure 2). However, as altered perfusion during ischemia and reperfusion is a hallmark of stroke, we assessed whether the [1-^{13}C]pyruvate delivery and uptake by cerebral tissue was altered (which could have masked the biochemical changes inherent to the penumbra) and performed additional analyses of our data.

Hyperpolarized [1-^{13}C]pyruvate delivery was significantly elevated compared with the remote region, by an average of 27% ± 2.9% (Figure 3A). Moreover, the overall amount of [1-^{13}C]pyruvate metabolism, represented by the sum of the metabolic derivatives, namely, [1-^{13}C]lactate, [1-^{13}C]alanine, and ^{13}C-bicarbonate signal, also increased in the area of stroke (by 18% ± 1.7%, henceforth referred to as "ΣAUC_d," a sum of area under the curve). The relative amounts by which the ΣAUC_d signal and infused [1-^{13}C]pyruvate signal increased displayed no relation with one another following regression analysis, suggesting that ΣAUC_d was uncoupled from bulk [1-^{13}C]pyruvate delivery to the region affected by transient ischemia (Figure 3B; $R^2 = .005$).

To interpret the surprising result that [1-^{13}C]pyruvate delivery did not influence ΣAUC_d, we considered the extensive experimental literature examining pyruvate uptake and metabolism in the cerebral tissue. In the healthy brain, the rate of pyruvate metabolism is uptake-limited by the presence of the BBB (27, 32). Pyruvate is taken up across the BBB via either MCT1 or MCT2 (33), or slow, unsaturable diffusion processes (27, 32). Previous work modeling hyperpolarized [1-^{13}C]pyru-

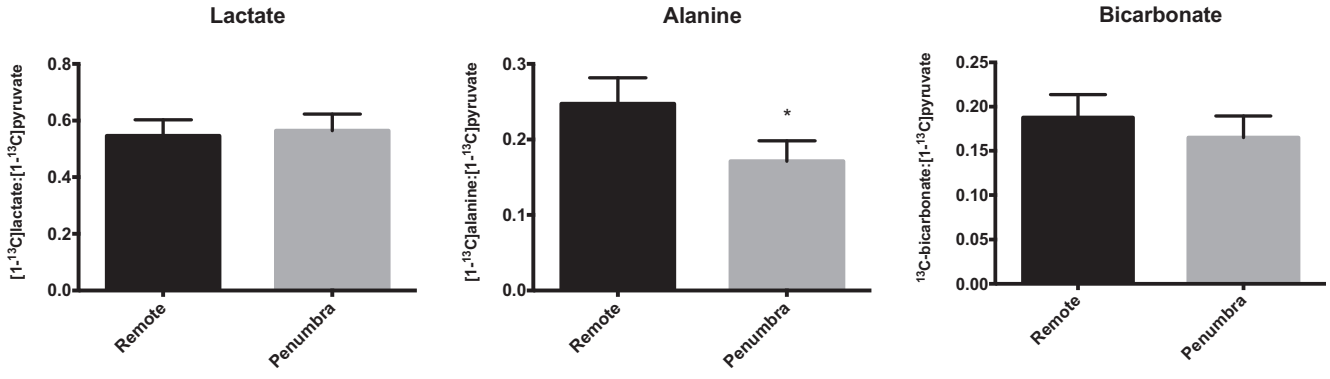

Figure 2. Production of each metabolic derivative of hyperpolarized [1-^{13}C]pyruvate, normalized to hyperpolarized [1-^{13}C]pyruvate signal. This data normalization method is most commonly used to account for differences in polarization and tracer delivery in the literature.

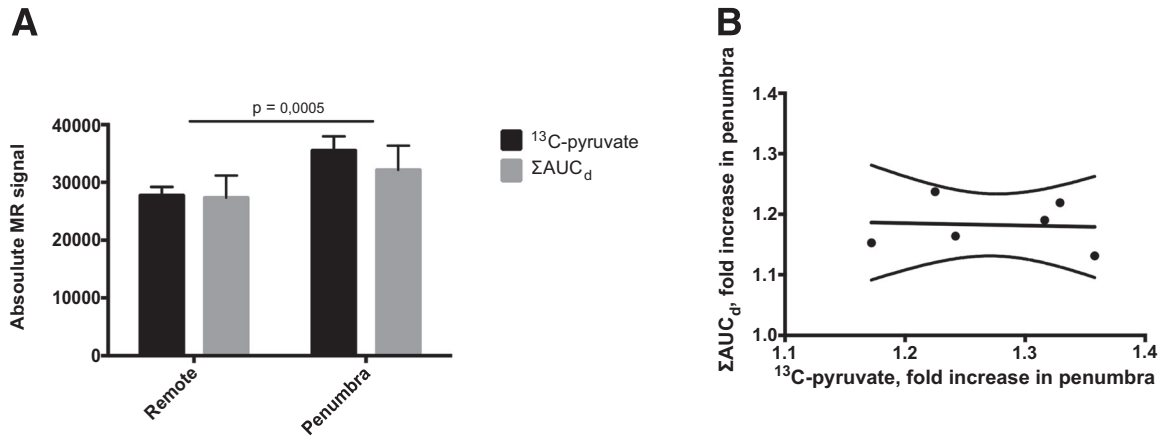

Figure 3. Hyperpolarized [1-^{13}C]pyruvate delivery and uptake are altered independently between remote region and the penumbra. Absolute signals measured from [1-^{13}C]pyruvate itself, and ΣAUC_d, on magnetic resonance (MR) images (A). Because all measurements were made simultaneously in symmetrical regions of the brain, there is no need to account for differences in polarization or dosing. *Interaction term*: remote-to-penumbra × normalization, $P = .01$. Although both parameters were increased in the penumbra, the relative increase in the [1-^{13}C]pyruvate signal showed no relationship with the relative increase in the ΣAUC_d (B). This suggests that a separate mechanism was responsible for the increase in the ΣAUC_d, independent of the increase in the local tracer.

vate uptake into healthy brain concluded that tracer transport through the BBB was 30- to 100-fold slower than its lactate dehydrogenase (LDH)-mediated conversion to [1-^{13}C]lactate, and, therefore, virtually all [1-^{13}C]pyruvate MR signals were localized in the extracellular space, with [1-^{13}C]pyruvate taken up into cells rapidly converted into its metabolic derivatives (29).

Taken together, these results and our observations suggest that, 1) although [1-^{13}C]pyruvate delivery to the penumbra appeared to have increased, changes to [1-^{13}C]pyruvate uptake across the BBB were driven by an independent mechanism(s); 2) the parameter of ΣAUC_d best reflected the rate of [1-^{13}C]pyruvate cellular uptake and thus the amounts of [1-^{13}C]pyruvate that could access the intracellular enzymes; and 3) practically speaking, because of the likelihood of altered [1-^{13}C]pyruvate delivery in stroke that may not affect cellular uptake across the rate-limiting BBB, normalizing metabolic data to [1-^{13}C]pyruvate signal may mask intracellular changes to enzyme activities that reflect pathophysiological status.

Lactate Production is Increased in Ischemic Penumbra

We removed normalization to [1-^{13}C]pyruvate signal and examined the absolute MR signal measured from each individual metabolite. Absolute [1-^{13}C]alanine and ^{13}C-bicarbonate signals remained unchanged between the 2 regions. [1-^{13}C]lactate signal was increased by 33% ± 7.9% in the penumbra. We then isolated the intracellular changes to enzymatic activity by normalizing the production of each metabolic derivative by the parameter of ΣAUC_d (as described above).

As shown in Figure 4, the conversion of hyperpolarized [1-^{13}C]pyruvate to [1-^{13}C]lactate increased by 16% in the pen-

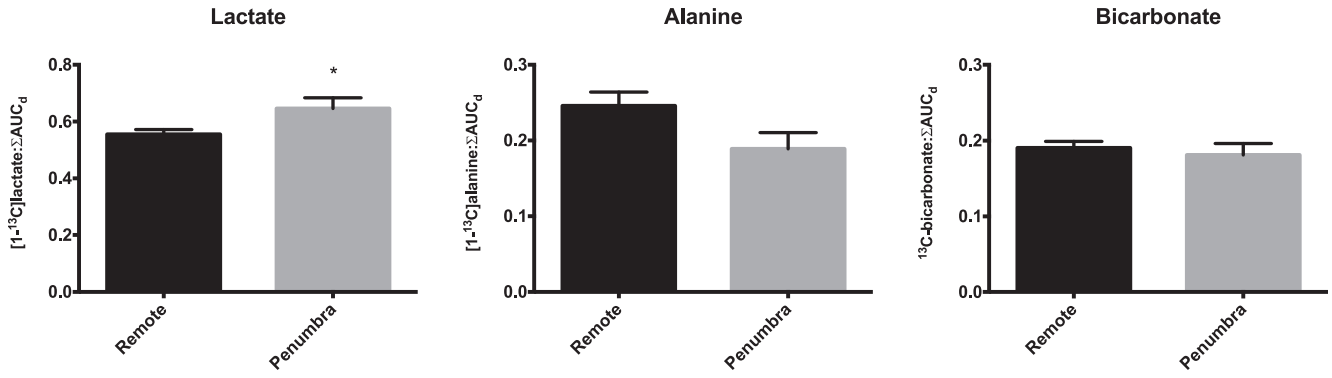

Figure 4. Production of each metabolic derivative of hyperpolarized [1-^{13}C]pyruvate, normalized to the parameter of ΣAUC_d, which best reflects tracer uptake across the blood–brain barrier (BBB).

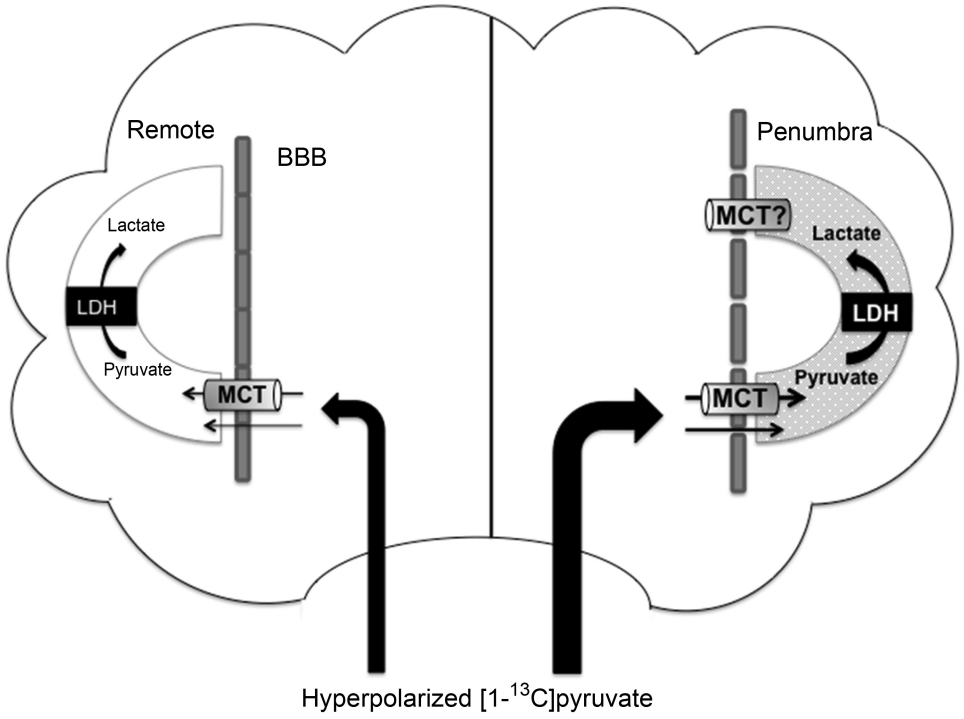

Figure 5. An illustration describing our proposed paradigm for the capacity of hyperpolarized [1-^{13}C] pyruvate to independently assess perfusion, tracer uptake across the BBB (possibly mediated by the monocarboxylate transporters [MCTs]), and metabolic reprogramming in a single experiment. The relative weights of each process between remote and penumbra regions are based upon the results we observed in this study, 18 hours following an ET-1-induced ischemic stroke. However, in stroke, all 3 parameters change over time, with each having the ability to predict patient outcomes. Assessing each parameter is essential for interpreting metabolic imaging data.

umbra (56% ± 1% of ΣAUC_d in the remote region and 65% ± 3% in the penumbra). This alteration was largely compensated for by reduced [1-^{13}C]alanine production (25% ± 1% of ΣAUC_d was converted to alanine in the remote region, yet only 19% ± 2% in the penumbra; $P = .056$). The conversion of hyperpolarized [1-^{13}C]pyruvate to ^{13}C-bicarbonate by the mitochondrial Pyruvate dehydrogenase enzyme complex (PDC) remained unaffected.

Can Hyperpolarized [1-^{13}C]Pyruvate Offer a "One-Stop Shop" to Report on Hemodynamics, BBB, and/or Enzyme Kinetics in Ischemic Stroke?

The aim of this study to provide a proof-of-concept that hyperpolarized MRI using [1-^{13}C]pyruvate can detect the metabolic reprogramming characteristic of ischemic penumbra (6-8, 15-18) was accomplished. Following infusion of hyperpolarized [1-^{13}C]pyruvate and spectroscopic image acquisition, we observed a significant 33% increase in absolute [1-^{13}C]lactate signal in the penumbra compared with that in a remote region. However, to interpret our enzymatic data, it was also essential to analyze alterations in tracer delivery and uptake. The alteration to [1-^{13}C]lactate production was obscured when routine normalization to absolute [1-^{13}C]pyruvate signal was performed. Upon normalization to cerebral tissue [1-^{13}C]pyruvate uptake (here ΣAUC_d), we observed a 16% increase in penumbral [1-^{13}C]lactate production. Thus, it seems likely that approximately half of increased [1-^{13}C]lactate signal reflected LDH-mediated [1-^{13}C]pyruvate/[1-^{13}C]lactate exchange because of increased LDH activity and/or intracellular lactate (20). The other half of [1-^{13}C]lactate signal may have simply reflected increased substrate provision to intracellular LDH.

Beyond providing a proof-of-concept, our results raise a number of questions regarding cerebral hyperpolarized tracer delivery and uptake whose answers will be essential to interpret metabolic imaging data in patients with stroke. Figure 5 shows a schematic illustration of the physiological processes hyperpolarized [1-^{13}C]pyruvate must experience between its point of infusion and its ultimate metabolic conversion into [1-^{13}C]lactate, which as follows: (1) delivery by blood flow/perfusion; (2) uptake across the BBB; and (3) enzymatic conversion. Our intention is that this illustration will assist in optimizing future investigations assessing metabolism following stroke in translational models, as all 3 of these parameters can change over time and each can predict patient outcomes.

The first step, of course, is delivery of the tracer by bulk blood flow and perfusion to the brain and particularly the penumbra. Recognizing reduced perfusion is critical for stroke diagnosis, and its rapid restoration is fundamental for treatment. Paradoxically, hyperemia in border zones and following reperfusion is also a well-known phenomenon, although the etiology and prognostic implications are unclear (34, 35). In this study, hyperpolarized [1-^{13}C]pyruvate MRI detected hyperemia 18 hours following ET-1-induced ischemic stroke. In future, correlating hyperpolarized results with quantitative perfusion imaging methods, such as arterial spin labeling or first-pass gadolinium-enhanced MRI, will be essential for characterizing metabolic tracer delivery to the region of interest, and perhaps to validate the use of hyperpolarized [1-^{13}C]pyruvate itself for reporting on regional perfusion in the brain.

[1-^{13}C]pyruvate cellular uptake and thus ΣAUC_d could increase in the penumbra because of BBB disruption, increased MCT expression, or a combination of both. Gadolinium-enhanced fluid-attenuated inversion recovery images (acquired several hours after gadolinium infusion) have indicated that one-third of patients with stroke experience BBB disruption

within 24 hours of ischemic stroke, and that this finding of "hyperintense acute reperfusion" in patients with stroke indicated a higher risk of hemorrhagic transformation and worse clinical outcome (36, 37). Studies performed in rodent stroke models suggested acutely increased expression of MCT1 and MCT2, starting as early as 1 hour after occlusion (38, 39), indicating that saturable MCT-mediated pyruvate uptake may well have been increased at our 18 hour time point. Future experimental studies would benefit from examining ΣAUC_d alongside spatiotemporal alterations in MCT isoform expression and in vivo Michaelis–Menten-type activity (40).

Correlation of [1-^{13}C]lactate production with the absolute concentrations of intracellular lactate, as well as rates at which irreversible tissue damage occurs, will be essential to determine if hyperpolarized [1-^{13}C]lactate imaging can predict the evolution of an ischemic lesion. In theory, the volume of tissue producing more [1-^{13}C]lactate because of LDH-mediated exchange should indicate the volume of penumbra, whereas the intensity of LDH-mediated [1-^{13}C]lactate production may indicate the regional severity of the occlusion; thus, the treatment window is important, during which reperfusion should be performed. These advances will be facilitated by using imaging methods described here in large, translational animal models of stroke, where increased relative spatial resolution is possible.

Its important to note that this study was performed solely with standard ^{1}H–T2-weighted imaging in combination with hyperpolarized ^{13}C MR. This imaging-focused approach limits the interpretation of the results. Further studies using advanced ^{1}H imaging methods for hemodynamic and diffusion changes associated with stroke, alongside biochemical assays to quantify the metabolic alterations, are needed to elucidate the exact mechanisms.

Clinical Significance

There is an urgent need in the neuroimaging community to validate a noninvasive marker for evaluation of ischemic penumbra, to guide reperfusion decisions, and to accurately select patients for clinical trials of neuroprotective drugs and delayed reperfusion strategies (6). By targeting the aberrant increase in tissue lactate levels that distinguishes penumbra from necrotic core and remote tissue, hyperpolarized ^{13}C MRI with [1-^{13}C]pyruvate shows potential to rapidly and noninvasively characterize both the size and stability of ischemic penumbra following stroke.

This study also opens the possibility of using other hyperpolarized tracers to identify viable and nonviable tissue following ischemic stroke. Experimentally, assessment of ATP levels and pH is considered as the most reliable invasive measurement for necrotic core and penumbra (6, 9, 15-18): the volume of tissue acidosis indicates the outer border of ischemic penumbra, and the inner region of ATP depletion below a certain level is indicative of the necrotic core. Hyperpolarized ^{13}C MRI can noninvasively detect both of these metabolic changes. Hyperpolarized ^{13}C-fumarate offers a positive contrast marker for necrosis via its conversion to ^{13}C-malate in the presence of cell membrane rupture only (41), and ^{13}C-malate production correlates with ATP depletion following myocardial infarction (42). Moreover, hyperpolarized ^{13}C-bicarbonate equilibrates with (13) CO_2 in the extracellular space in a pH-dependent manner, and imaging their ratio yields a measurement of pH (43). One can envision a combined imaging approach, in which the volume of a ^{13}C-malate image, indicative of necrosis, is subtracted from the outer boundary of a pH (9) or [1-^{13}C]lactate image to provide a positive contrast imaging for the necrotic core and ischemic penumbra.

The imaging methods commonly used to assess stroke often require multiple scans to individually assess the physiological status of tissue experiencing heterogeneous perfusion conditions (ie, positron emission tomography perfusion–metabolism mismatch studies, MR perfusion– diffusion mismatch). The time required for multiple scans can be prohibitive in patients with stroke who must always be treated as quickly as possible. Cunningham et al. have reported that a hyperpolarized ^{13}C pyruvate scan adds 10 minutes to the duration of a routine clinical MRI assessment (44), suggesting that the technology could be implemented to acquire images following stroke within the limited treatment window. In future, the potential for a single technique– hyperpolarized ^{13}C MRI–to rapidly and noninvasively assess multiple aspects of cerebral physiology could be crucial for ensuring a comprehensive assessment of the penumbra.

ACKNOWLEDGMENTS

Henrik Vestergaard is acknowledged for his laboratory assistance.

Disclosures: No disclosures to report.

Conflict of Interest: None reported.

REFERENCES

1. American Stroke Association. Let's Talk About Ischemic Stroke. 2015.
2. Hacke W, Kaste M, Bluhmki E, Brozman M, Dávalos A, Guidetti D, Larrue V, Lees KR, Medeghri Z, Machnig T, Schneider D, von Kummer R, Wahlgren N, Toni D; ECASS Investigators. Thrombolysis with alteplase 3 to 4.5 hours after acute ischemic stroke. N Engl J Med. 2008;359(13):1317–1329.
3. Saver JL, Goyal M, Bonafe A, Diener HC, Levy EI, Pereira VM, Albers GW, Cognard C, Cohen DJ, Hacke W, Jansen O, Jovin TG, Mattle HP, Nogueira RG, Siddiqui AH, Yavagal DR, Baxter BW, Devlin TG, Lopes DK, Reddy VK, du Mesnil de Rochemont R, Singer OC, Jahan R; SWIFT PRIME Investigators. Stent-retriever thrombectomy after intravenous t-PA vs. t-PA alone in stroke. N Engl J Med. 2015;372(24):2285–2295.
4. O'Collins VE, Macleod MR, Donnan GA, Horky LL, van der Worp BH, Howells DW. 1,026 experimental treatments in acute stroke. Ann Neurol. 2006;59(3):467–477.
5. Heiss WD. Experimental evidence of ischemic thresholds and functional recovery. Stroke. 1992;23(11):1668–1672.
6. Heiss WD. The ischemic penumbra: correlates in imaging and implications for treatment of ischemic stroke. The Johann Jacob Wepfer award 2011. Cerebrovasc Dis. 2011;32(4):307–320.
7. Arnberg F, Grafström J, Lundberg J, Nikkhou-Aski S, Little P, Damberg P, Mitsios N, Mulder J, Lu L, Söderman M, Stone-Elander S, Holmin S. Imaging of a clinically relevant stroke model: glucose hypermetabolism revisited. Stroke. 2015;46(3):835–842.

8. Ginsberg MD, Reivich M, Giandomenico A, Greenberg JH. Local glucose utilization in acute focal cerebral ischemia: local dysmetabolism and diaschisis. Neurology. 1977;27(11):1042–1048.
9. Moseley ME. Molecular imaging and stroke. Stroke, 2009;40(3 Suppl): S30–S33.
10. Barber PA, Darby DG, Desmond PM, Yang Q, Gerraty RP, Jolley D, Donnan GA, Tress BM, Davis SM. Prediction of stroke outcome with echoplanar perfusion- and diffusion-weighted MRI. Neurology. 1998;51(2):418–426.
11. Butcher KS, Parsons M, MacGregor L, Barber PA, Chalk J, Bladin C, Levi C, Kimber T, Schultz D, Fink J, Tress B, Donnan G, Davis S; EPITHET Investigators. Refining the perfusion-diffusion mismatch hypothesis. Stroke. 2005;36(6):1153–1159.
12. Zaro-Weber O, Moeller-Hartmann W, Heiss WD, Sobesky J. The performance of MRI-based cerebral blood flow measurements in acute and subacute stroke compared with 15O-water positron emission tomography: identification of penumbral flow. Stroke. 2009;40(7):2413–2421.
13. Davis SM, Donnan GA. MR mismatch and thrombolysis: appealing but validation required. Stroke. 2009;40(8):2910.
14. Wardlaw JM. Surrogate outcomes: a cautionary note. Stroke. 2009;40(4): 1029–1031.
15. Siesjö BK. Cell damage in the brain: a speculative synthesis. J Cereb Blood Flow Metab. 1981;1(2):155–185.
16. Behar KL, Rothman DL, Hossmann KA. NMR spectroscopic investigation of the recovery of energy and acid-base homeostasis in the cat brain after prolonged ischemia. J Cereb Blood Flow Metab. 1989;9(5):655–665.
17. Plum F. What causes infarction in ischemic brain?: The Robert Wartenberg Lecture. Neurology. 1983;33(2):222–233.
18. Chang LH, Shimizu H, Abiko H, Swanson RA, Faden AI, James TL, Weinstein PR. Effect of dichloroacetate on recovery of brain lactate, phosphorus energy metabolites, and glutamate during reperfusion after complete cerebral ischemia in rats. J Cereb Blood Flow Metab. 1992;12(6):1030–1038.
19. Ardenkjaer-Larsen JH, Fridlund B, Gram A, Hansson G, Hansson L, Lerche MH, Servin R, Thaning M, Golman K. Increase in signal-to-noise ratio of >10,000 times in liquid-state NMR. Proc Natl Acad Sci U S A. 2003;100(18):10158–10163.
20. Day SE, Kettunen MI, Gallagher FA, Hu DE, Lerche M, Wolber J, Golman K, Ardenkjaer-Larsen JH, Brindle KM. Detecting tumor response to treatment using hyperpolarized 13C magnetic resonance imaging and spectroscopy. Nat Med. 2007;13(11):1382–1387.
21. Golman K, in't Zandt R, Thaning M. Real-time metabolic imaging. Proc Natl Acad Sci U S A. 2006;103(30):11270–11275.
22. Nelson SJ, Kurhanewicz J, Vigneron DB, Larson PE, Harzstark AL, Ferrone M, van Criekinge M, Chang JW, Bok R, Park I, Reed G, Carvajal L, Small EJ, Munster P, Weinberg VK, Ardenkjaer-Larsen JH, Chen AP, Hurd RE, Odegardstuen LI, Robb FJ, Tropp J, Murray JA. Metabolic imaging of patients with prostate cancer using hyperpolarized [1-(1)(3)C]pyruvate. Sci Transl Med. 2013;5(198): 198ra108.
23. Schroeder MA, Swietach P, Atherton HJ, Gallagher FA, Lee P, Radda GK, Clarke K, Tyler DJ. Measuring intracellular pH in the heart using hyperpolarized carbon dioxide and bicarbonate: a 13C and 31P magnetic resonance spectroscopy study. Cardiovasc Res. 2010;86(1):82–91.
24. O h-Ici D, Wespi P, Busch J, Wissmann L, Krajewski M, Weiss K, Sigfridsson A, Messroghli D, Kozerke S. Hyperpolarized metabolic MR imaging of acute myocardial changes and recovery after ischemia-reperfusion in a small-animal model. Radiology. 2016;278(3):742–751.
25. Albers MJ, Bok R, Chen AP, Cunningham CH, Zierhut ML, Zhang VY, Kohler SJ, Tropp J, Hurd RE, Yen YF, Nelson SJ, Vigneron DB, Kurhanewicz J. Hyperpolarized 13C lactate, pyruvate, and alanine: noninvasive biomarkers for prostate cancer detection and grading. Cancer Res. 2008;68(20):8607–8615.
26. Nielsen PM, Laustsen C, Bertelsen LB, Qi H, Mikkelsen E, Kristensen ML3, Nørregaard R, Stødkilde-Jørgensen H. In situ lactate dehydrogenase activity - a novel renal cortical imaging biomarker of tubular injury? Am J Physiol Renal Physiol, 2016; 312(3): F465–F473. [Epub ahead of print]. doi: 10.1152/ajprenal.00561.2015
27. Pardridge WM. Brain metabolism: a perspective from the blood-brain barrier. Physiol Rev. 1983;63(4):1481–1535.
28. Hurd RE, Yen YF, Mayer D, Chen A, Wilson D, Kohler S, Bok R, Vigneron D, Kurhanewicz J, Tropp J, Spielman D, Pfefferbaum A. Metabolic imaging in the anesthetized rat brain using hyperpolarized [1-13C] pyruvate and [1-13C] ethyl pyruvate. Magn Reson Med. 2010;63(5):1137–1143.
29. Hurd RE, Yen YF, Tropp J, Pfefferbaum A, Spielman DM, Mayer D. Cerebral dynamics and metabolism of hyperpolarized [1-(13C]pyruvate using time-resolved MR spectroscopic imaging. J Cereb Blood Flow Metab. 2010;30(10):1734–1741.
30. Windle V, Szymanska A, Granter-Button S, White C, Buist R, Peeling J, Corbett D. An analysis of four different methods of producing focal cerebral ischemia with endothelin-1 in the rat. Exp Neurol. 2006;201(2):324–334.
31. Ansari S, Azari H, Caldwell KJ, Regenhardt RW, Hedna VS, Waters MF, Hoh BL, Mecca AP. Endothelin-1 induced middle cerebral artery occlusion model for ischemic stroke with laser Doppler flowmetry guidance in rat. J Vis Exp. 2013;(72).
32. Miller LP, Oldendorf WH. Regional kinetic constants for blood-brain barrier pyruvic acid transport in conscious rats by the monocarboxylic acid carrier. J Neurochem. 1986;46(5):1412–1416.
33. Halestrap AP, Wilson MC. The monocarboxylate transporter family–role and regulation. IUBMB Life. 2012;64(2):109–119.
34. Olsen TS, Larsen B, Skriver EB, Herning M, Enevoldsen E, Lassen NA. Focal cerebral hyperemia in acute stroke. Incidence, pathophysiology and clinical significance. Stroke. 1981;12(5):598–607.
35. Heiss WD, Graf R, Rosner G. Postischemic hyperemia. In: Manabe H, Zweifach BW, Messmer K, eds. Microcirculation in Circulatory Disorders. Springer-Verlag; 1988: 277–279. Osaka, Japan.
36. Henning EC, Latour LL, Warach S. Verification of enhancement of the CSF space, not parenchyma, in acute stroke patients with early blood-brain barrier disruption. J Cereb Blood Flow Metab. 2008;28(5):882–886.
37. Yang Y, Rosenberg GA. Blood-brain barrier breakdown in acute and chronic cerebrovascular disease. Stroke. 2011;42(11):3323–3328.
38. Rosafio K, Castillo X, Hirt L, Pellerin L. Cell-specific modulation of monocarboxylate transporter expression contributes to the metabolic reprograming taking place following cerebral ischemia. Neuroscience. 2016;317:108–120.
39. Zhang F, Vannucci SJ, Philp NJ, Simpson IA. Monocarboxylate transporter expression in the spontaneous hypertensive rat: effect of stroke. J Neurosci Res. 2005;79(1-2):139–145.
40. Schroeder MA, Atherton HJ, Cochlin LE, Clarke K, Radda GK, Tyler DJ. The effect of hyperpolarized tracer concentration on myocardial uptake and metabolism. Magn Reson Med. 2009;61(5):1007–1014.
41. Gallagher FA, Kettunen MI, Hu DE, Jensen PR, Zandt RI, Karlsson M, Gisselsson A, Nelson SK, Witney TH, Bohndiek SE, Hansson G, Peitersen T, Lerche MH, Brindle KM. Production of hyperpolarized [1,4-13C2]malate from [1,4-13C2]fumarate is a marker of cell necrosis and treatment response in tumors. Proc Natl Acad Sci U S A. 2009;106(47):19801–19806.
42. Nielsen PM, Eldirdiri A, Bertelsen LB, Jørgensen HS, Ardenkjaer-Larsen JH, Laustsen C. Fumarase activity: an in vivo and in vitro biomarker for acute kidney injury. Sci Rep. 2017;7:40812.
43. Gallagher FA, Kettunen MI, Day SE, Hu DE, Ardenkjaer-Larsen JH, Zandt Ri, Jensen PR, Karlsson M, Golman K, Lerche MH, Brindle KM. Magnetic resonance imaging of pH in vivo using hyperpolarized 13C-labelled bicarbonate. Nature. 2008;453(7197):940–943.
44. Cunningham CH, Lau JY, Chen AP, Geraghty BJ, Perks WJ, Roifman I, Wright GA, Connelly KA. Hyperpolarized 13C metabolic MRI of the human heart: Initial Experience. Circ Res. 2016;119(11):1177–1182.